Energy & Environmental Science

Cite this: *Energy Environ. Sci.*, 2012, **5**, 8923

www.rsc.org/ees

COMMUNICATION

In situ probe of photocarrier dynamics in water-splitting hematite (α-Fe_2O_3) electrodes†

Zhuangqun Huang,‡[a] Yongjing Lin,[b] Xu Xiang,[c] William Rodríguez-Córdoba,[a] Kenneth J. McDonald,[d] Karl S. Hagen,[a] Kyoung-Shin Choi,[d] Bruce S. Brunschwig,[e] Djamaladdin G. Musaev,[f] Craig L. Hill,[a] Dunwei Wang[b] and Tianquan Lian*[a]

Received 27th June 2012, Accepted 9th August 2012
DOI: 10.1039/c2ee22681b

The spectra and dynamics of photogenerated electrons and holes in excited hematite (α-Fe_2O_3) electrodes are investigated by transient absorption (from visible to infrared and from femto- to microseconds), bias-dependent differential absorption and Stark spectroscopy. Comparison of results from these techniques enables the assignment of the spectral signatures of photogenerated electrons and holes. Under the pulse illumination conditions of transient absorption (TA) measurement, the absorbed photon to electron conversion efficiency (APCE) of the films at 1.43 V (*vs.* reversible hydrogen electrode, RHE) is 0.69%, significantly lower than that at AM 1.5. TA kinetics shows that under these conditions, >98% of the photogenerated electrons and holes have recombined by 6 μs. Although APCE increases with more positive bias (from 0.90 to 1.43 V *vs.* RHE), the kinetics of holes up to 6 μs show negligible change, suggesting that the catalytic activity of the films is determined by holes with longer lifetimes.

[a]*Department of Chemistry, Emory University, Atlanta, Georgia 30322, USA. E-mail: tlian@emory.edu; Fax: +1 404 727 6586; Tel: +1 404 727 6649*
[b]*Department of Chemistry, Merkert Chemistry Center, Boston College, 2609 Beacon Street, Chestnut Hill, Massachusetts 02467, USA*
[c]*State Key Laboratory of Chemical Resource Engineering, Beijing University of Chemical Technology, Beijing 100029, PR China*
[d]*Department of Chemistry, Purdue University, West Lafayette, Indiana 47907, USA*
[e]*Beckman Institute, California Institute of Technology, Pasadena, California, 91125, USA*
[f]*Cherry L. Emerson Center for Scientific Computation, Emory University, Atlanta, Georgia 30322, USA*

† Electronic supplementary information (ESI) available: Experimental details, transient spectra, bias-dependent differential UV-Vis absorption spectra, the estimate of maximum transient electric field, FTIR spectra, and the fitting parameters for the kinetics. See DOI: 10.1039/c2ee22681b

‡ Present address: Joint Center for Artificial Photosynthesis, California Institute of Technology, 1200 East California Boulevard, Pasadena, CA 91125.

Hematite (α-Fe_2O_3) is an intensively studied photoanode material for water oxidation due to its suitable bandgap (2.1 eV), abundance, environmental compatibility, and stability under photoelectrochemical (PEC) conditions in various neutral and alkaline electrolytes.[1–8] Intense current research efforts have been aimed at optimizing PEC performance by controlling the hematite structure, morphology, and surface chemistry and understanding fundamental charge carrier dynamics.[2,3,7,9,10] Despite these efforts, little is known about the spectral signatures and dynamics of photogenerated electrons and holes in these electrodes under water oxidation conditions.[11] An early study by radiolysis showed that reduced hematite colloidal particles have a broad absorption band above 500 nm due to the conduction band or trapped electrons.[12] Using this assignment, transient absorption (TA) spectroscopic studies have reported short-lived (<100 picoseconds) photocarriers in these materials.[13–20] In contrast to these earlier findings, more recent studies have identified a long-lived (>microseconds) absorption band at 580 nm due to photogenerated holes[21,22] in nanoporous hematite films with reported high incident-photon-to-electron-conversion-efficiency (IPCE).[23] Thus, both the spectral assignment and dynamics of photocarriers remain unclear due, at least in part, to the limited temporal (less than

Broader context

Solar water splitting using semiconductor photoelectrodes is an attractive approach to harvest solar energy and store it in chemical forms. Among the photoelectrodes studied, hematite stands out for its high theoretical efficiency, chemical stability and abundance. Despite the potentially high achievable efficiency, the progress in performance improvement is impeded by the lack of fundamental understanding of the photocarrier dynamics within hematite and at the solid–liquid junctions. In this work, we employed transient absorption and bias-dependent differential absorption spectroscopy to study the spectral signatures and dynamics of photogenerated electrons and holes in hematite electrodes under water oxidation conditions. Similar studies can be extended to other solar-to-fuel conversion materials.

one nanosecond or longer than microseconds) and spectral ranges of these previous studies. In this communication, we report a TA study on hematite electrodes under water oxidation conditions with broadband spectral (visible to mid-IR) and temporal (femto- to micro-seconds) ranges. In conjunction with spectral-electrochemical and absorbed photon-to-electron conversion efficiency (APCE) measurements, these *in situ* TA studies provide clear spectral assignment of photogenerated electrons and holes, reveal their dynamics, and show that ultrafast electron–hole recombination is the main efficiency limiting factor under our experimental conditions.

Fig. 1 shows the UV-Vis absorption spectrum of a 30 nm hematite thin film grown by atomic layer deposition on a fluorine-doped tin oxide (FTO) coated glass (MTI, TCO 15). The absorption features result from the ligand field d–d and the direct O2p → Fe4s (>3.5 eV) transitions.[24–27] Also shown in Fig. 1 is the IPCE spectrum measured using a solar simulator coupled with a monochromator (Oriel cornerstone 260) at 1.43 V (*vs.* reversible hydrogen electrode, RHE) in 1 M NaOH. An IPCE of 25% is obtained at ~400 nm, comparable to the highest reported values.[23] The high IPCE of these films can be attributed to the small film thickness, which facilitates scavenging of holes by solution and collection of the photogenerated electrons.[28,29] The mismatch between the IPCE and absorption spectra is due to the difference between the short hole diffusion length (2–4 nm)[30] and the long photon penetration depth (from 120 to 46 nm for photon wavelengths from 550 to 450 nm).[2,31]

Transient absorption spectra of hematite films at 100 fs to 25 μs after 400 nm excitation were recorded. Details of the sub-picosecond and sub-nanosecond spectrometers used for the measurement can be found in the ESI.† TA spectra at selected delay time windows are shown in Fig. 2 and more spectra at other delay times can be found in Fig. S1.† The TA spectra show an ultrafast bleach recovery below ~525 nm and a decay of absorption bands above ~550 nm within the first 30 ps. After 30 ps, the transient spectra consist of bleach bands at 425 and 525 nm, and absorption bands at 470, 515 and 570 nm. These features show negligible dependence on the applied bias or solvent environment (air, water, methanol, ethanol, NaOH aqueous solution). As shown in Fig. S1 and S2,† similar TA spectra are observed in thin films of different thickness grown by ALD,[28] nanoparticle films prepared by electrochemical deposition,[32,33] and colloidal particle suspensions,[34] indicating that these features originate from the intrinsic absorption of electrons and holes in these materials.

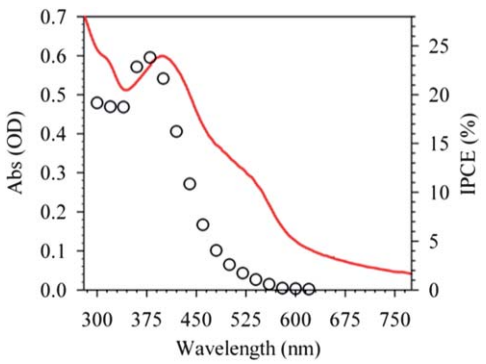

Fig. 1 UV-Vis absorption (red line) and the incident-photon-to-electron conversion efficiency (IPCE, black open circles) spectra of a 30 nm hematite thin film grown by atomic layer deposition. IPCE measurement conditions: 1.43 V *vs.* RHE, simulated AM 1.5 solar illumination, 1 M NaOH.

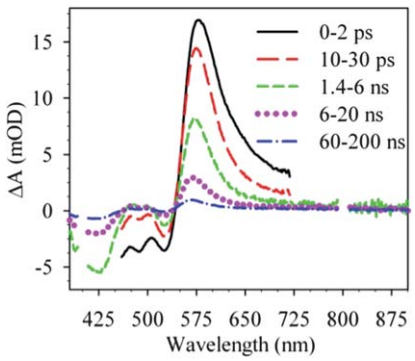

Fig. 2 Transient absorption spectra of a hematite thin film (30 nm) after 400 nm excitation. The film is exposed to air. Each spectrum is an average of 30–130 spectra at different delay times within the indicated time windows. The spectra after 1 ns were recorded with a spectrometer with a broader probe light. See Fig. S1† for more detailed spectra.

However, the relative amplitudes of the bands and the kinetics vary in these samples.

To assign the transient spectral signatures, we measured the UV-Vis absorption spectra under different biases in a three-electrode PEC cell. Bias dependent differential spectra were constructed by subtracting off the spectrum at open circuit (Fig. S5†). The hematite films were stable under low bias, but degradation occurred when the bias was more negative than −1.1 V *vs.* Ag/AgCl. Selected difference spectra (0.43 V and −1 V *vs.* Ag/AgCl) together with the UV-Vis spectrum are scaled and compared to the TA spectra at 1 ns in Fig. 3. The difference spectra at −1 V show a negative peak (bleach) at 400 nm, a positive band at ~580 nm and a broad absorption feature at wavelength >600 nm. Under a negative bias, electrons accumulate on the hematite surface at the solid–liquid junction. The filling of these electrons in the originally empty levels can reduce the transition probability of these levels, which results in bleach of the ground state transitions in the difference spectrum. Therefore the bleach at 400 nm can be assigned to the state filling induced bleach of the ground state absorption band. In addition, the excess electrons in the accumulation layer lead to new optical absorption features at 580 nm and

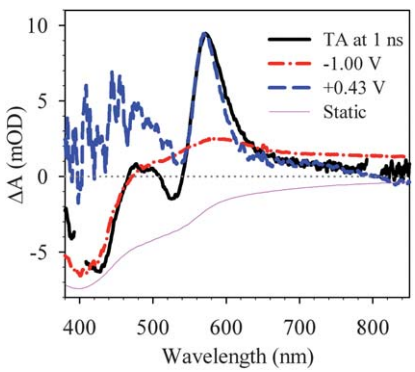

Fig. 3 Comparison of transient absorption (TA) spectrum (black solid line), differential static absorption spectra at −1.00 (red dashed-dotted line) and 0.43 V (blue short dashed line, *vs.* Ag/AgCl in 1 M NaOH), and steady-state UV-Vis absorption spectrum (pink thin solid line, inverted) of hematite thin films. The TA spectrum is taken at 1 ns after 400 nm excitation of a film exposed to the air. These spectra have been scaled for better comparison.

longer wavelengths, consistent with the broad absorption observed in reduced hematite particles generated by radiolysis.[12] Both bleach and the absorption features become smaller as the applied bias becomes less negative. When the bias is ≥0.15 V *vs.* Ag/AgCl, new absorption features, particularly, a sharp band at ~570 nm, are formed. As shown in Fig. 3, this absorption feature is in good agreement with the TA peak at 570 nm. Under positive bias, the electron occupancy in or near the valence band is reduced, a condition that is similar to the photogeneration of holes. Therefore the feature at 570 nm can be assigned to the absorption of holes in the hematite. This is consistent with a reported long-lived (μs-to-ms) hole absorption band at ~580 nm in nanoporous hematite films, whose lifetime was shown to decrease dramatically with the addition of a hole scavenger and to increase in the presence of water oxidation catalyst or under positive biases.[21,35]

Photoinduced separation of electrons and holes can generate a transient electric field in the material, which modulates the energy of ground and excited states, resulting in changes in its absorption spectrum.[36–38] To examine this effect, we have also performed a steady-state Stark effect measurement, in which the spectral change resulting from an applied external electric field is recorded. In our system, assuming a perfect distribution of the photocarriers in a parallel-plate capacitor (Fig. S6†), the maximum transient electric field is estimated to be $\sim 4.8 \times 10^7$ V m^{-1} (see ESI†). The actual field strength is likely to be smaller due to random charge distribution and the short-hole diffusion length (2–4 nm).[30] The application of a DC field of 2.0×10^7 V m^{-1} to the ALD sample leads to a spectral change of <0.2 mOD, which is over 50 times smaller than the TA signal at 1 ns (~10 mOD). Therefore, the transient Stark effect contributes negligibly to the observed TA signals.

The transient kinetics monitored at different wavelengths are shown in Fig. 4. These kinetic traces can be fitted by multiple exponential decay functions and the fitting parameters are shown in Table S1.† The signal at 675 nm, which is dominated by the absorption of electrons, decays by ~88% within 10 ps, consistent with kinetics reported by Zhang *et al.*[11,20,39] A multiple exponential fit (Table S1†) of the data yields a fast decay component with 0.2 ps time constant and 73% of the total amplitude. The kinetics at 570 nm, which is dominated by the absorption of holes, shows a smaller amplitude (55%) of a similarly fast decay component and much longer lived components. To further investigate the origin of the initial ultrafast decay component, we also probe the free carrier intra-subband transitions at 2000 cm^{-1}.[40] The kinetics (Fig. 4) is dominated by the ultrafast decay component (0.2 ps and 94%). If this fast decay is due to electron–hole recombination, one would expect the same kinetics at different wavelengths. The observed wavelength dependent kinetics suggests that the ultrafast decay component can be attributed to the trapping and cooling of free electrons, although some contribution due to charge recombination cannot be excluded.

Following the initial ultrafast process, the kinetics at 570 nm shows a slow component that exists beyond 6 μs, the longest delay time probed in this study. This is consistent with the long-lived (μs-to-ms) signal at ~580 nm observed previously.[21,35] Due to the slow water oxidation reaction, only these long-lived photocarriers are responsible for water splitting.

In order to correlate transient kinetics to the photoelectrochemical water oxidation performance, we simultaneously measured the *in situ* carrier dynamics and photocurrent in a PEC cell. The photocurrent results from the illumination of the 400 nm pump and the broadband white light probe used in the transient study. As shown in Fig. S7 and S8,† when the bias of the electrode is tuned from 0.90 to 1.43 V (*vs.* RHE), the photocurrent increases rapidly. This trend is similar to the *I–V* curve recorded using simulated AM 1.5 solar illumination, but the current amplitude is much smaller.[28] The averaged APCE is estimated to be 0.69% at 1.43 V (*vs.* RHE), much smaller than that shown in Fig. 1 and reported in the literature.[28] This difference can be attributed to the intense laser pulse used in this measurement. The estimated peak power density is 100 nJ/150 fs/(400 μm)^2 = 10^{11} mW cm^{-2} or 10^9 AM 1.5 suns. The pulse excitation generates large transient concentrations of electrons and holes, which enhance the charge recombination rate.

The transient kinetics at 570 nm monitored at different bias voltages are compared in Fig. 5. Surprisingly, these hole kinetics show negligible change within this range of applied biases. The amplitude of the remaining hole signal at 6 μs is <2% of the initial value, consistent with the low APCE under these conditions. It is likely that the differences in the hole lifetime may appear after 6 μs. Indeed Durrant and co-workers[21,22] reported a long-lived (μs-to-ms) absorption band at 580 nm that can be correlated with the photocatalytic performance of the cell. Furthermore, change of APCE from ~0.01% at 0.90 V to 0.69% at 1.43 V corresponds to a long-lived hole amplitude of 0.001 and 0.069 mOD. The difference is likely smaller than the sensitivity of this measurement. Therefore, future measurements will require improved sensitivity and lower excitation

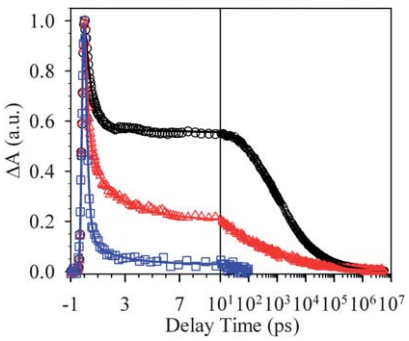

Fig. 4 Normalized transient kinetics of hematite thin films monitored at 570 nm (black open circles) and 675 nm (red triangles), and 2000 cm^{-1} (blue squares) after 400 nm excitation. The solid lines are multiple-exponential fit to the data. The films are exposed to the air.

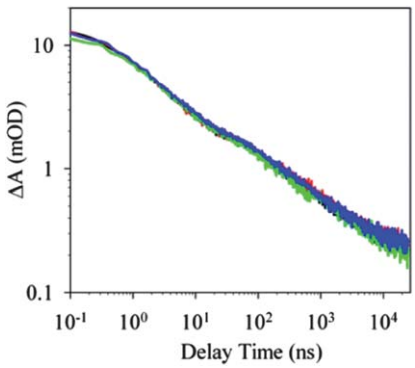

Fig. 5 *In situ* transient kinetics of hematite monitored at 570 nm after 400 nm excitation under different biases: −0.90 (black), 1.10 (red), 1.26 (green) and 1.43 V (blue, *vs.* RHE).

power, as demonstrated in previous works.[21–23] This finding also highlights the challenges in correlating the IPCE performance with ultrafast transient absorption measurement.[11,20,39]

Conclusions

In conclusion, transient absorption spectra of hematite electrodes from the visible to the near IR and from femtoseconds to microseconds have been recorded. By comparison with the static absorption spectra of the films recorded under electron and hole accumulation conditions, the spectral signatures of electrons and holes in the TA spectra have been assigned. These spectral features are similar in hematite materials of different morphologies which are prepared by different methods, although the kinetics are different. Under pulse illumination conditions of TA spectroscopy, the measured APCE at 1.43 V (*vs.* RHE) is 0.69%, much smaller than that at AM 1.5. More than 98% of the photo-generated holes have already decayed by 6 μs, suggesting that electron–hole recombination is the main efficiency limiting factor under our experimental conditions. Furthermore, while the APCE increases with the applied bias (from 0.90 to 1.43 V *vs.* RHE), the TA kinetics of holes up to 6 μs show negligible bias-dependence, suggesting that the catalytic activity of the electrodes is determined by holes with lifetimes longer than 6 μs.

Acknowledgements

DGM, CLH and TL acknowledge the support of the U.S. Department of Energy, Office of Basic Energy Sciences, Solar Photochemistry Program (DE-FG02-07ER-15906); financial support for BSB was provided by an NSF Center for Chemical Innovation (CHE-0802907) at Caltech. YJ and DW are supported by NSF through a CAREER Award (DMR-1055762). KJM and KSC acknowledge the support by the U.S. Department of Energy, Office of Basic Energy Sciences, Solar Photochemistry Program (DE-FG02-05ER15752); steady-state Stark spectral data were collected at the Molecular Materials Research Center of the Beckman Institute of the California Institute of Technology. ZH is grateful to the productive discussion with the members of Lewis group.

Notes and references

1 S. D. Tilley, M. Cornuz, K. Sivula and M. Gratzel, *Angew. Chem., Int. Ed.*, 2010, **49**, 6405.
2 K. Sivula, F. Le Formal and M. Gratzel, *ChemSusChem*, 2011, **4**, 432.
3 J. W. Sun, D. K. Zhong and D. R. Gamelin, *Energy Environ. Sci.*, 2010, **3**, 1252.
4 T. V. L. Lindgren, H. Wang and S.-E. Lindquist, *Chem. Phys. Nanostruct. Semicond.*, 2003, 83.
5 M. P. Dare-Edwards, J. B. Goodenough, A. Hamnett and P. R. Trevellick, *J. Chem. Soc., Faraday Trans. 1*, 1983, **79**, 2027.
6 D. K. Zhong and D. R. Gamelin, *J. Am. Chem. Soc.*, 2010, **132**, 4202.
7 E. Khon, A. Mereshchenko, A. N. Tarnovsky, K. Acharya, A. Klinkova, N. N. Hewa-Kasakarage, I. Nemitz and M. Zamkov, *Nano Lett.*, 2011, **11**, 1792.
8 Y. Lin, G. Yuan, S. Sheehan, S. Zhou and D. Wang, *Energy Environ. Sci.*, 2011, **4**, 4862.
9 H. Dotan, K. Sivula, M. Gratzel, A. Rothschild and S. C. Warren, *Energy Environ. Sci.*, 2011, **4**, 958.
10 B. Klahr, S. Gimenez, F. Fabregat-Santiago, J. Bisquert and T. W. Hamann, *Energy Environ. Sci.*, 2012, **5**, 7626.
11 D. A. Wheeler, G. Wang, Y. Ling, Y. Li and J. Z. Zhang, *Energy Environ. Sci.*, 2012, **5**, 6682.
12 N. M. Dimitrijevic, D. Savic, O. I. Micic and A. J. Nozik, *J. Phys. Chem.*, 1984, **88**, 4278.
13 G. Xiong, A. G. Joly, G. P. Holtom, C. M. Wang, D. E. McCready, K. M. Beck and W. P. Hess, *J. Phys. Chem. B*, 2006, **110**, 16937.
14 V. A. Nadtochenko, N. N. Denisov, V. Y. Gak, F. E. Gostev, A. A. Titov, O. M. Sarkisov and V. V. Nikandrov, *Russ. Chem. Bull.*, 2002, **51**, 457.
15 A. G. Joly, G. Xiong, C. M. Wang, D. E. McCready, K. M. Beck and W. P. Hess, *Appl. Phys. Lett.*, 2007, **90**, 103504.
16 A. G. Joly, J. R. Williams, S. A. Chambers, G. Xiong, W. P. Hess and D. M. Laman, *J. Appl. Phys.*, 2006, **99**, 053521.
17 Y. P. He, Y. M. Miao, C. R. Li, S. Q. Wang, L. Cao, S. S. Xie, G. Z. Yang, B. S. Zou and C. Burda, *Phys. Rev. B: Condens. Matter Mater. Phys.*, 2005, **71**, 125411.
18 L. M. Fu, Z. Y. Wu, X. C. Ai, J. P. Zhang, Y. X. Nie, S. S. Xie, G. Z. Yang and B. S. Zou, *J. Chem. Phys.*, 2004, **120**, 3406.
19 H. M. Fan, G. J. You, Y. Li, Z. Zheng, H. R. Tan, Z. X. Shen, S. H. Tang and Y. P. Feng, *J. Phys. Chem. C*, 2009, **113**, 9928.
20 N. J. Cherepy, D. B. Liston, J. A. Lovejoy, H. M. Deng and J. Z. Zhang, *J. Phys. Chem. B*, 1998, **102**, 770.
21 S. R. Pendlebury, M. Barroso, A. J. Cowan, K. Sivula, J. W. Tang, M. Gratzel, D. Klug and J. R. Durrant, *Chem. Commun.*, 2011, **47**, 716.
22 J. W. Tang, A. J. Cowan, J. R. Durrant and D. R. Klug, *J. Phys. Chem. C*, 2011, **115**, 3143.
23 A. Kay, I. Cesar and M. Gratzel, *J. Am. Chem. Soc.*, 2006, **128**, 15714.
24 D. M. Sherman and T. D. Waite, *Am. Mineral.*, 1985, **70**, 1262.
25 D. M. Sherman, *Phys. Chem. Miner.*, 1985, **12**, 161.
26 Y. Matsumoto, *J. Solid State Chem.*, 1996, **126**, 227.
27 J. B. Goodenough, *Prog. Solid State Chem.*, 1971, **5**, 145.
28 Y. J. Lin, S. Zhou, S. W. Sheehan and D. W. Wang, *J. Am. Chem. Soc.*, 2011, **133**, 2398.
29 Y. Lin, Y. Xu, M. T. Mayer, Z. I. Simpson, G. McMahon, S. Zhou and D. Wang, *J. Am. Chem. Soc.*, 2012, **134**, 5508.
30 J. H. Kennedy and K. W. Frese, *J. Electrochem. Soc.*, 1977, **124**, C130.
31 R. F. G. Gardner, F. Sweett and D. W. Tanner, *J. Phys. Chem. Solids*, 1963, **24**, 1183.
32 R. L. Spray and K. S. Choi, *Chem. Mater.*, 2009, **21**, 3701.
33 R. L. Spray, K. J. McDonald and K.-S. Choi, *J. Phys. Chem. C*, 2011, **115**, 3497.
34 Y. T. He, J. M. Wan and T. Tokunaga, *J. Nanopart. Res.*, 2008, **10**, 321.
35 M. Barroso, A. J. Cowan, S. R. Pendlebury, M. Gratzel, D. R. Klug and J. R. Durrant, *J. Am. Chem. Soc.*, 2011, **133**, 14868.
36 H. M. Zhu, N. H. Song and T. Q. Lian, *J. Am. Chem. Soc.*, 2010, **132**, 15038.
37 S. Ardo, Y. Sun, A. Staniszewski, F. N. Castellano and G. J. Meyer, *J. Am. Chem. Soc.*, 2010, **132**, 6696.
38 S. G. Boxer, *J. Phys. Chem. B*, 2009, **113**, 2972.
39 G. M. Wang, Y. C. Ling, D. A. Wheeler, K. E. N. George, K. Horsley, C. Heske, J. Z. Zhang and Y. Li, *Nano Lett.*, 2011, **11**, 3503.
40 J. I. Pankove, *Optical Processes in Semiconductors*, New York, Dover, 1975.

